British Journal of Cancer

ARTICLE

Translational Therapeutics

Characterisation of a novel KRAS G12C inhibitor ASP2453 that shows potent anti-tumour activity in KRAS G12C-mutated preclinical models

Ayako Nakayama[1]✉, Takeyuki Nagashima[1], Yoshihiro Nishizono[1], Kazuyuki Kuramoto[1], Kenichi Mori[1], Kazuya Homboh[1], Masatoshi Yuri[1] and Masashi Shimazaki[2]

BACKGROUND: *KRAS* is one of the most frequently mutated oncogenes in various cancers, and several novel KRAS G12C direct inhibitors are now in clinical trials. Here, we characterised the anti-tumour efficacy of ASP2453, a novel KRAS G12C inhibitor, in preclinical models of KRAS G12C-mutated cancer.

METHODS: We evaluated the in vitro and in vivo activity of ASP2453, alone or in combination with targeted agents and immune checkpoint inhibitors, in KRAS G12C-mutated cancer cells and xenograft models. We also assessed pharmacological differences between ASP2453 and AMG 510, another KRAS G12C inhibitor, using an SPR assay, washout experiments and an AMG 510-resistant xenograft model.

RESULTS: ASP2453 potently and selectively inhibited KRAS G12C-mediated growth, KRAS activation and downstream signalling in vitro and in vivo, and improved the anti-tumour effects of targeted agents and immune checkpoint inhibitors. Further, ASP2453 had more rapid binding kinetics to KRAS G12C protein and showed more potent inhibitory effects on KRAS activation and cell proliferation after washout than AMG 510. ASP2453 also induced tumour regression in an AMG 510-resistant xenograft model.

CONCLUSIONS: ASP2453 is a potential therapeutic agent for KRAS G12C-mutated cancer. ASP2453 showed efficacy in AMG 510-resistant tumours, even among compounds with the same mode of action.

British Journal of Cancer (2022) 126:744–753; https://doi.org/10.1038/s41416-021-01629-x

BACKGROUND

Kirsten rat sarcoma viral oncogene homologue (KRAS) is a member of the Ras family of proteins and one of the most frequently mutated oncogenes in various cancers. Ras is a small GTPase that functions as a molecular switch to turn on or off receptor tyrosine kinase (RTK) signal transduction by binding to guanosine triphosphate (GTP) or guanosine diphosphate (GDP). Following growth factor stimulation of RTK, guanine nucleotide exchange factors (GEFs) such as Son of Sevenless (SOS) promote activation of Ras by catalysing the exchange of GDP for GTP. GTP binding changes the conformation of Ras, which promotes interaction with effector proteins including Raf, phosphatidylinositol 3-kinase (PI3K) and Ral guanine nucleotide dissociation stimulators (Ral-GDS), and activates downstream signalling pathways such as mitogen-activated protein kinase (MAPK) and PI3K, which regulate cell proliferation, differentiation and survival. RAS-GTP is inactivated when GTP is converted to GDP by its GTPase activity, which is accelerated by GTPase activating proteins (GAPs) that catalyse GTP hydrolysis. Ras inactivation reduces downstream signalling [1–3]. Thus, Ras plays an important role in cell proliferation, differentiation and survival.

Most *KRAS* missense mutations occur at codon 12 in the P-loop [4] and cause resistance to GAP-catalysed hydrolysis and accelerate downstream signalling [3, 5, 6]. The KRAS G12C mutation is found in ~13% of lung adenocarcinoma, 3% of colorectal cancer, 3% of pancreatic cancer and other solid tumours [4, 7]. In lung adenocarcinoma, the leading cause of cancer death worldwide [8, 9], KRAS G12C is the most common type of amino acid substitution among KRAS mutations and is known as the smoking-associated mutation due to G to T transversion by tobacco carcinogens [10, 11]. The KRAS G12C mutation is independently associated with worse disease-free survival (DFS) and overall survival (OS) compared with other KRAS mutations or wild-type (WT) in resected lung adenocarcinoma [12]. Therefore, inhibitors targeting KRAS G12C may be potential therapeutic agents for these cancers.

Recent studies have reported a new allosteric pocket on KRAS G12C in the switch-II region, which is exposed only in the GDP-bound state, and inhibitors that covalently bind to the cysteine at residue 12 (Cys12) of KRAS [13, 14]. Additionally, novel KRAS G12C direct inhibitors were recently tested in Phase 1/2/3 clinical trials. FDA-approved drug AMG 510, known as sotorasib, developed by

[1]Drug Discovery Research, Astellas Pharma Inc., Tsukuba-shi, Ibaraki, Japan. [2]Astellas Research Institute of America LLC, Northbrook, IL, USA. ✉email: ayako.nakayama@astellas.com

Received: 1 July 2021 Revised: 25 October 2021 Accepted: 3 November 2021
Published online: 18 November 2021

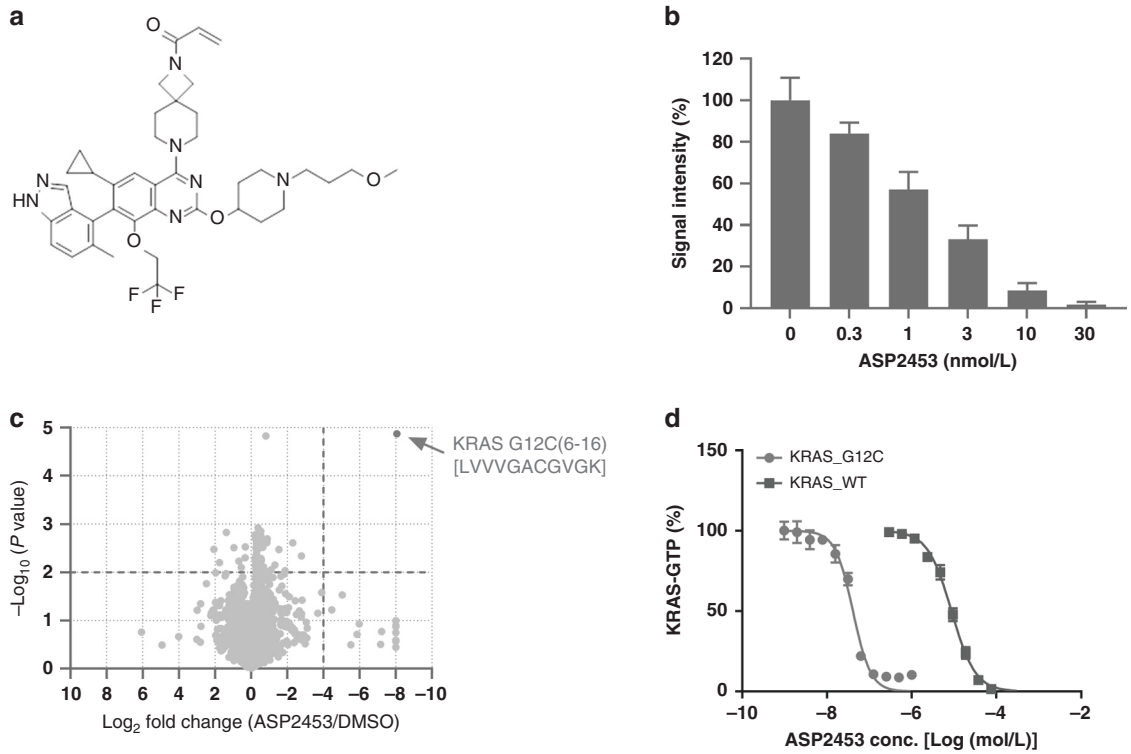

Fig. 1 ASP2453 is a potent, selective and covalent KRAS G12C inhibitor. a Chemical structure of ASP2453. **b** Interaction between ASP2453 and KRAS G12C (mean ± SD). **c** ASP2453, among the proteome in NCI-H1373 cells, selectively binds to KRAS G12C after treatment for 2 h at 30 nmol/L. **d** Inhibitory activity of ASP2453 on SOS-mediated KRAS G12C-Raf or KRAS WT-Raf interactions (mean ± SEM, three independent experiments).

Amgen [15, 16] and MRTX849, known as adagrasib, developed by Mirati Therapeutics [17] covalently bind to Cys12 of KRAS G12C protein and lock it in the inactive GDP-bound state. Oral treatment with these compounds shows anti-tumour effects in preclinical models. The first-in-human study of AMG 510 showed that 19 out of 59 (32.2%) patients with non-small cell lung cancer (NSCLC), 3 out of 44 (7.1%) patients with colorectal cancer and 4 out of 28 (14.3%) with other tumours achieved confirmed partial response (PR) [18]. In the MRTX849 study, 23 out of 51 (45%) patients with NSCLC and 3 out of 18 (17%) patients with colon cancer achieved an objective response, and some patients with other solid tumours achieved PR [19, 20]. In addition, a Phase 1 trial of GDC-6036 developed by Genentech is currently under way [21]. Based on reports from first-in-human studies, these KRAS G12C inhibitors exhibit clinical efficacy in KRAS G12C-mutated patients. Although these compounds have similar modes of action, it is unclear whether their pharmacological differences impact their anti-tumour activity and acquisition of drug resistance.

In this report, we characterised the preclinical profile of ASP2453 in KRAS G12C-mutated cancer. We demonstrated that ASP2453 covalently interacts and selectively binds to KRAS G12C. ASP2453 potently and selectively inhibits KRAS G12C-mediated cell proliferation, KRAS activation and downstream signalling in vitro. ASP2453 also induces anti-tumour activity and enhances the anti-tumour effects of MAPK kinase (MEK), epidermal growth factor receptor (EGFR) and checkpoint inhibitors in various KRAS G12C-dependent xenograft models. Compared to AMG 510, ASP2453 has more rapid binding kinetics and more potent and durable inhibitory effects on KRAS activation and cell proliferation after washout. Furthermore, ASP2453 induces tumour regression in AMG 510-resistant tumours. Our data indicate that ASP2453 displays therapeutic potential for KRAS G12C-mutated cancer. Thus, differences in potency and binding kinetics may affect anti-tumour efficacy, even among covalent KRAS G12C inhibitors of the same class.

METHODS

Reagents

(+)−1-{7-[6-Cyclopropyl-2-{[1-(3-methoxypropyl)piperidin-4-yl]oxy}−7-(5-methyl-1*H*-indazol-4-yl)−8-(2,2,2-trifluoroethoxy)quinazolin-4-yl]−2,7-diazaspiro[3.5]non-2-yl}prop-2-en-1-one (ASP2453, Fig. 1a, WO/2018/143315, Ex.38), AMG 510 [15] and trametinib were synthesised in-house. Erlotinib was purchased from Cayman CHEMICAL (Ann Arbor, MI, USA). ASP2453, AMG 510, erlotinib and trametinib were dissolved in dimethyl sulfoxide (DMSO) for in vitro experiments. For in vivo experiments, ASP2453 and AMG 510 were suspended in 6% (2-hydroxypropyl)-β-cyclodextrin (HP-CD; Sigma-Aldrich, St. Louis, MO, USA) solution, erlotinib was suspended in 10% HP-CD, and trametinib was suspended in 0.5% Methyl Cellulose 400 Solution (0.5% MC; FUJIFILM Wako Pure Chemical Corporation, Osaka, Japan).

Recombinant proteins

Biotinylated AviTag KRAS G12C protein (1–185) and biotinylated AviTag KRAS WT protein (1–185) were expressed in *Escherichia coli*, loaded with GDP (Sigma-Aldrich) and purified in-house. SOS and glutathione *S*-transferase (GST)-tagged c-Raf were expressed in *Escherichia coli*, and purified in-house. EGF recombinant human protein solution was purchased from ThermoFisher Scientific (Waltham, MA, USA).

Cell lines

NCI-H1373, NCI-H358, NCI-H23, NCI-H1792, NCI-H1355, HCT-15, HCT 116, A549, A375, AsPC-1, and CT26.WT cells were purchased from American Type Culture Collection (Manassas, VA, USA); MIA PaCa-2 and LU65 cells were purchased from RIKEN BRC (Ibaraki, Japan); NCI-H727 cells were purchased from European Collection of Authenticated Cell Cultures (Porton Down, UK); and SW837 cells were purchased from Japanese Collection of Research Bioresources Cell Bank (Osaka, Japan). MIA PaCa-2 and NCI-H727 cells were cultured in RPMI 1640 medium (Sigma-Aldrich). Other cell lines were cultured according to the manufacturer's guidelines. All media were supplemented with 10% heat-inactivated fetal bovine serum and penicillin-streptomycin (50 U/mL and 50 µg/mL; ThermoFisher Scientific). All cell lines were incubated at 37 °C in 5% CO_2. The cell lines used in this

study were not authenticated in our laboratory but were purchased from providers of authenticated cell lines and stored at early passages in a central cell bank at Astellas Pharma Inc. The experiments were conducted using low-passage cultures of these stocks with *mycoplasma* testing.

Cell-free assay

ASP2453 was incubated with 400 nmol/L biotinylated AviTag KRAS G12C (1–185, GDP) or KRAS WT (1–185, GDP). These mixtures of ASP2453 and KRAS G12C/WT protein were added to 1.3 μmol/L SOS and 130 nmol/L GST-tagged c-Raf containing 4 μmol/L GTP. After incubating for 1 h, 120 nmol/L ULight-anti-GST (PerkinElmer, Waltham, MA, USA) and 100 ng/mL LANCE Eu-W1024 Streptavidin (PerkinElmer) was added. The fluorescence intensity of each sample at 620 and 665 nm was measured using an EnVision Multilabel Reader (PerkinElmer) at an excitation wavelength of 337 nm.

In-cell ELISA assay

NCI-H1373 or A375 cells were seeded in 384-well clear flat-bottom plates at 2×10^4 or 1×10^4 cells/well, respectively, and incubated overnight. The following day, the cells were treated with ASP2453 or trametinib (1 μmol/L) for 2 h. After fixation and permeabilization, extracellular signal-regulated kinase 1 and 2 phosphorylation (p-ERK 1/2) levels were measured using an ELISA assay. p-ERK 1/2 rabbit mAb (#4370; Cell Signaling Technology, Danvers, MA, USA) and goat anti-rabbit IRDye 800CW (LI-COR Biosciences, Lincoln, NE, USA) were used as the primary antibody and secondary antibody, respectively, and fluorescence signals were quantified using Aerius (LI-COR Biosciences). The signal in the DMSO-treated group was used to indicate 100% and that in the trametinib-treated group was used to indicate 0%.

In vitro cell growth assay

The cells were seeded in low attachment 96-well round-bottom white plates (Sumitomo Bakelite, Tokyo, Japan) at 1×10^3 cells/well and incubated overnight. The following day, the cells were treated with ASP2453 for 6 days. Cell viability was determined using a CellTiter-Glo 2.0 Assay (Promega, Madison, WI, USA). For washout experiments, the cells were seeded in 96-well flat-bottom plates at 1×10^3 cells/well and incubated overnight. The following day, the cells were treated with ASP2453 or AMG 510 for 6 or 24 h. After treatment, each well was washed 3 times with medium and incubated for 6 days. Cell viability was determined using a CellTiter-Glo 2.0 Assay.

Immunoblotting and RAF-RBD pulldown assay

Cells were seeded and incubated overnight. The following day, the cells were treated with ASP2453 or AMG 510 at the indicated concentrations and times. Cells were lysed with lysis buffer, and levels of p-Akt, Akt, p-ERK 1/2, ERK 1/2, p-S6, S6, KRAS and β-actin protein were detected by immunoblotting. The active form of KRAS was detected using an RAF-RBD pulldown assay. The cell lysate was mixed with GST magnetic beads (ThermoFisher Scientific) and the GST-tagged Ras-binding domain (RBD) of Ras effector kinase Raf1 (GST-Raf-RBD; Cell Signaling Technology). After incubating for 1 h, the beads were eluted with SDS-PAGE sample buffer and the eluted complex was used to detect KRAS-GTP and GST-Raf-RBD. The eluted beads and lysate were separated by SDS-PAGE, transferred to a PVDF membrane, and blotted using primary and secondary antibodies. The chemiluminescent signal was detected and images were taken using an ImageQuant LAS 4000 (GE Healthcare Life Sciences, Chicago, IL, USA). KRAS (F234) antibody (sc-30) was purchased from Santa Cruz Biotechnology (Dallas, TX, USA); β-actin antibody (A1978) from Sigma-Aldrich; rabbit IgG HRP (18-8816-33) for GST and mouse IgG HRP (18-8817-33) for KRAS and β-actin from Rockland Immunochemicals (Limerick, PA, USA); and GST (#2625), p-Akt (#4060), Akt (#9272), ERK 1/2 (#9102), p-S6 (#4858), S6 (#2317) and rabbit IgG HRP (#7074) antibodies from Cell Signaling Technology.

In vivo anti-tumour studies in xenografts

All animal experimental procedures were approved by the Institutional Animal Care and Use Committee of Astellas Pharma Inc., Tsukuba Research Center, which is accredited by AAALAC International. Mice were housed in individually ventilated cages, depending on group size (5–8 mice per cage) and maintained on water and a standard diet throughout the experimental procedures. For cancer cell line-based xenograft (CDX) studies, NCI-H1373, MIA PaCa-2, NCI-H358 and A375 cells were subcutaneously inoculated into the flank of 4-weeks-old male nude mice (Balb/c nu/nu; Charles River Laboratories Japan, Inc., Kanagawa, Japan) at 3×10^6 cells/0.1 mL (Matrigel [Corning, Corning, NY, USA]:phosphate-buffered saline [PBS] = 1:1)/mouse and allowed to grow. For patient-derived xenograft (PDX)-based studies conducted at Charles River Discovery Research Services Germany GmbH (Freiburg, Germany) or Xentech (Evry, France), each tumour was subcutaneously implanted into nude mice (NMRI nu/nu or Balb/c nu/nu, respectively; Envigo, Indianapolis, IN, USA) and allowed to grow.

The mice were randomised into treatment groups based on tumour volume and ASP2453, AMG 510, trametinib or erlotinib was administered orally once a day. Tumour volume was calculated using the formula length × $\text{width}^2 \times 0.5$.

Molecular modelling of ASP2453 and AMG 510 bound to KRAS G12C

The coordinates of KRAS G12C bound to ARS-1620 (Protein Data Bank [PDB] ID: 5V9U) [22] were selected as the template for modelling. While keeping the covalent region of ARS-1620 bound to KRAS G12C cysteine 12, the chemical structure of ARS-1620 was gradually changed to ASP2453 with iterative minimisation with each modification. The final model was generated by replacing the covalent region of ARS-1620 with that of ASP2453 and optimising the coordinates by energy minimisation. We constructed the molecular model of KRAS G12C bound to AMG 510 by superposing the backbone atoms of the published X-ray structure of KRAS G12C bound to AMG 510 (PDB ID: 6OIM) [15] over that of KRAS G12C bound to ASP2453 described above. The missing hydrogen atoms were added using the Protonate3D function in the modelling software MOE (Chemical Computing Group Inc., Montreal, QC, CA). Molecular visualisation and minimisation were performed using MOE.

Surface plasmon resonance (SPR) biosensor analysis

Biotinylated AviTag KRAS G12C (1–185, GDP) was immobilised on a Series S Sensor Chip SA (GE Healthcare Life Sciences) using immobilisation buffer (HBS-P+, 1 mmol/L DTT, 1 mmol/L $MgCl_2$ and 1 μmol/L GDP). ASP2453 and AMG 510 were diluted to 30 or 100 nmol/L using running buffer (HBS-P+, 1 mmol/L $MgCl_2$ and 1 μmol/L GDP) with a constant DMSO concentration of 2%, and then injected into the flow cells at a flow rate of 30 μL/min for 600 s (association), followed by running buffer for 90 s (dissociation). The association phase of each sensorgram was analysed by plotting response unit (RU) values normalised to the molecular weight of the compounds.

RESULTS

ASP2453 is a potent, selective and covalent KRAS G12C inhibitor

In a structure-based drug optimisation process, we identified ASP2453 as a potent KRAS G12C covalent inhibitor (Fig. 1a). To determine the selectivity of ASP2453, we performed a target engagement assay and cysteine selectivity profiling of KRAS G12C-mutated NCI-H1373 cells using LC–MS/MS to evaluate the covalent interaction between ASP2453 and KRAS G12C. After treatment of NCI-H1373 cells with ASP2453 for 2 h, ASP2453 showed dose-dependent interactions with KRAS G12C (Fig. 1b). Moreover, Cys12 of KRAS was the only peptide among 4783 cysteine-containing peptides that interacted with ASP2453 (Fig. 1c). The inhibitory activity of ASP2453 on the SOS-mediated interaction between KRAS and Raf was measured using TR-FRET. ASP2453 inhibited the SOS-mediated interaction between KRAS G12C and Raf in a concentration-dependent manner with an IC_{50} value of 40 nmol/L. This inhibition was 215-fold more potent than that against the interaction between KRAS WT and Raf (Fig. 1d, Supplementary Table S1). These results suggest that ASP2453 is a covalent and mutant-specific KRAS G12C inhibitor.

ASP2453 selectively inhibits KRAS signalling and proliferation of KRAS G12C-mutated cancer cells in vitro

ASP2453 dose-dependently and completely inhibited p-ERK 1/2, a downstream effector of KRAS, with an IC_{50} value of 2.5 nmol/L in NCI-H1373 cells, but not in KRAS WT A375 cells at doses up to

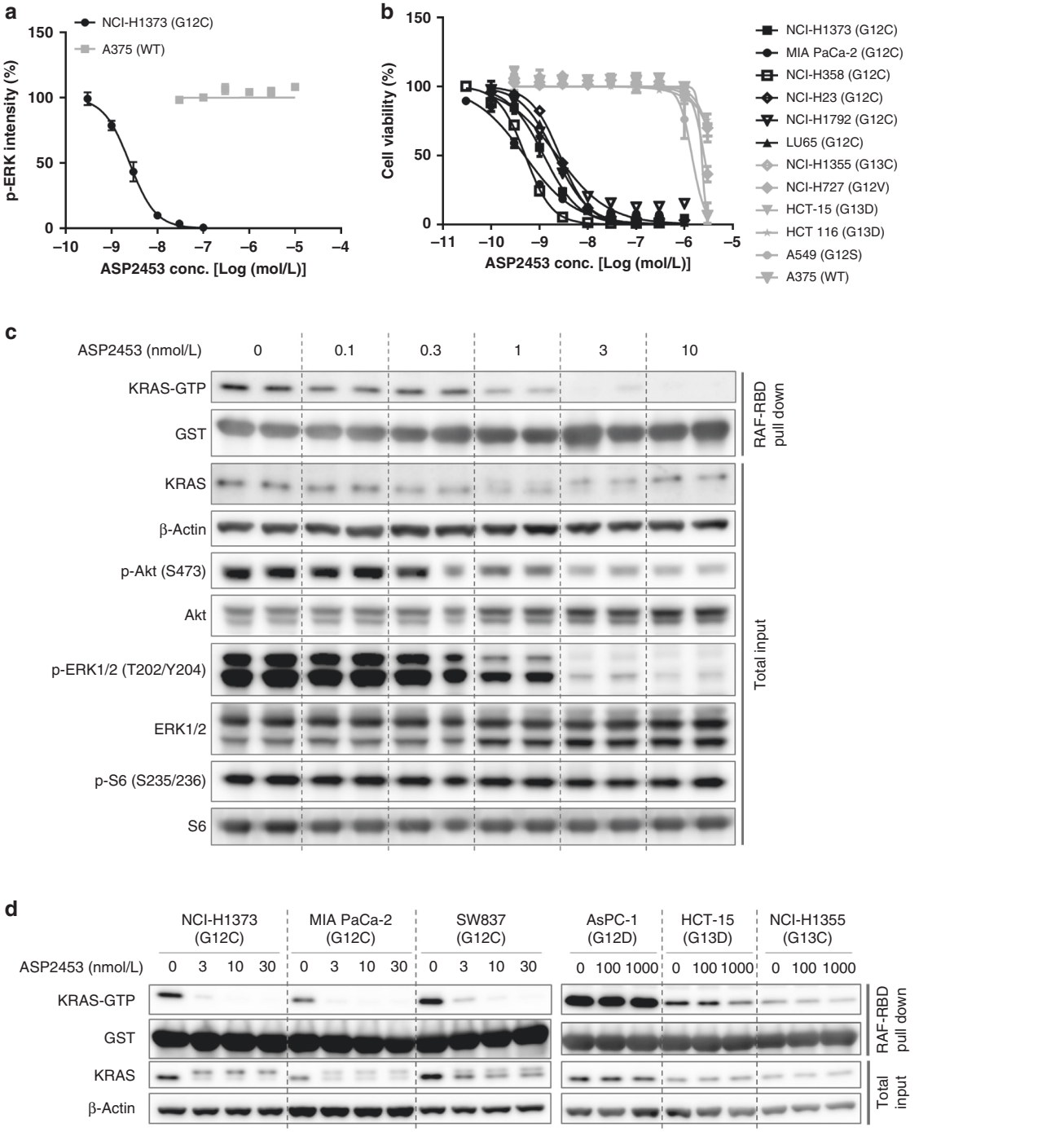

Fig. 2 ASP2453 selectively inhibits KRAS signalling and proliferation of KRAS G12C-mutated in cancer cells in vitro. a Inhibitory activity of ASP2453 on p-ERK 1/2 after treatment for 2 h (mean ± SEM, three independent experiments). **b** Inhibitory activity of ASP2453 on the proliferation of human cancer cells harbouring KRAS G12C mutations in 3D spheroid culture (mean ± SEM, three independent experiments). **c** Effect of ASP2453 on KRAS activation, KRAS mobility shift and downstream signals in NCI-H1373 cells after treatment for 2 h. **d** Effect of ASP2453 on KRAS activation and KRAS mobility shift in KRAS-mutated cell lines after treatment for 2 h.

10 μmol/L (Fig. 2a and Supplementary Table S1). To evaluate the inhibitory effects and selectivity of ASP2453 on cell proliferation, we investigated its anti-proliferative effects in various human cancer cell lines harbouring KRAS mutations or WT. ASP2453 inhibited the growth of cells harbouring KRAS G12C mutations with IC_{50} values below 3 nmol/L (Fig. 2b and Supplementary Table S2) in 3D spheroid cell culture. In contrast, ASP2453 did not inhibit the growth of cells harbouring other KRAS mutations or KRAS WT at 300 nmol/L (Fig. 2b and Supplementary Table S2).

We next investigated the inhibitory activity of ASP2453 on KRAS G12C-mediated signal transduction using RAF-RBD pulldown and immunoblotting. ASP2453 dose-dependently suppressed KRAS-GTP, p-Akt and p-ERK 1/2 in NCI-H1373 cells at concentrations starting from 1 nmol/L, which is approximately equal to the IC_{50} needed for growth inhibition (Fig. 2c). Further, ASP2453 induced the mobility shift of KRAS due to covalent binding to KRAS G12C protein similarly to other KRAS G12C covalent inhibitors [15, 17]. In MIA PaCa-2 cells, another KRAS G12C-mutated cell line, ASP2453 also suppressed

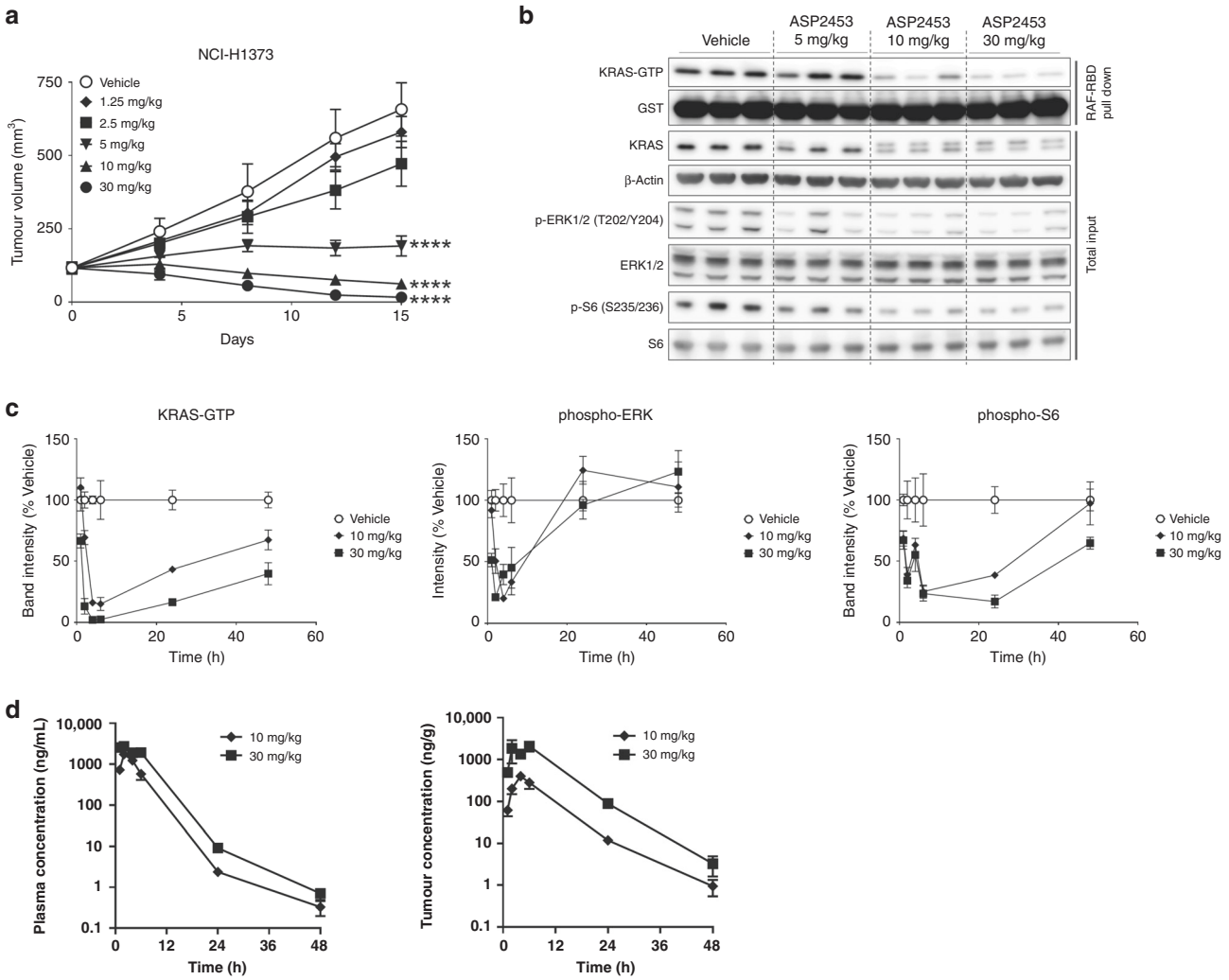

Fig. 3 Oral administration of ASP2453 induces anti-tumour activity in an NCI-H1373 xenograft model. a Anti-tumour activity of ASP2453 in a subcutaneous KRAS G12C-mutated NCI-H1373 xenograft model ($n = 5$ mice per group, mean ± SEM). ****$P < 0.0001$, Dunnett's multiple comparison test compared with vehicle. **b** Effect of ASP2453 on KRAS activation, KRAS mobility shift, p-ERK 1/2 and p-S6 in NCI-H1373 tumours at 6 h after administration of a single dose. **c** Pharmacodynamics of ASP2453 on KRAS-GTP, p-ERK 1/2 and p-S6 in NCI-H1373 tumours. Tumour samples were collected at 1, 2, 4, 6, 24 and 48 h after administration of a single dose ($n = 3$ mice per group, mean ± SEM). **d** Plasma and tumour concentrations of ASP2453. Plasma and tumour samples were collected at 1, 2, 4, 6, 24 and 48 h after administration of a single dose ($n = 3$ mice per group, mean ± SD).

KRAS-GTP, p-ERK 1/2 and p-S6 and induced the mobility shift of KRAS from the concentration of 3 nmol/L (Supplementary Fig. S1A, B). While effects of ASP2453 on suppression of KRAS-GTP and induction of the mobility shift of KRAS were observed in NCI-H1373, MIA PaCa-2 and SW837 KRAS G12C-mutated cell lines, they were not observed in AsPC-1, HCT-15 or NCI-H1355, other KRAS-mutated cell lines, at 100 nmol/L (Fig. 2d). Taken together, these results suggest that ASP2453 potently and selectively inhibits KRAS G12C-mediated KRAS activation, downstream signalling events such as ERK 1/2 phosphorylation, and cell proliferation.

ASP2453 induces tumour regression in KRAS G12C-mutated xenograft models in vivo

In vivo studies were conducted to examine the anti-tumour activity of ASP2453 in a subcutaneous xenograft model using NCI-H1373 cells. Once-daily oral administration of ASP2453 significantly and dose-dependently inhibited tumour growth, with 47% and 86% tumour regression observed at 10 and 30 mg/kg, respectively (Fig. 3a and Supplementary Table S3), without affecting body weight (Supplementary Fig. S2A). Single oral administration of ASP2453 suppressed KRAS-GTP and induced mobility shift of KRAS in tumours at 10 and 30 mg/kg, doses at which tumour regression was observed (Fig. 3b). ASP2453 also inhibited downstream signals from 5 mg/kg.

We next examined the pharmacokinetic and pharmacodynamic profiles of ASP2453 in the NCI-H1373 xenograft model to determine whether drug exposure was correlated with KRAS G12C inhibition. Maximum inhibition of KRAS activation, p-ERK 1/2 and p-S6 was observed at 4–6 h, 2–4 h, and 6 h, respectively, and suppression of KRAS-GTP was sustained for 48 h after a single oral dose of ASP2453 (Fig. 3c). The maximum concentration of ASP2453 was observed at 2 h in plasma, and at 4 h (10 mg/kg) or 6 h (30 mg/kg) in tumour (Fig. 3d and Supplementary Table S4). C_{max} and AUC_t values in plasma and tumour increased with increasing dose. These results show that inhibition of KRAS activation, p-ERK 1/2 and p-S6 is correlated with increasing intratumor concentrations of ASP2453.

To further assess the anti-tumour effects of ASP2453, we examined other subcutaneous pancreatic cancer MIA PaCa-2 CDX or PDX models. ASP2453 inhibited tumour growth or caused tumour regression in the MIA PaCa-2 pancreatic CDX model, the LXFA592 lung PDX model (Fig. 4a, b) and other PDX models derived from lung, pancreatic or colon cancer patients (Supplementary Table S3). In contrast, ASP2453 did not inhibit tumour growth in the KRAS

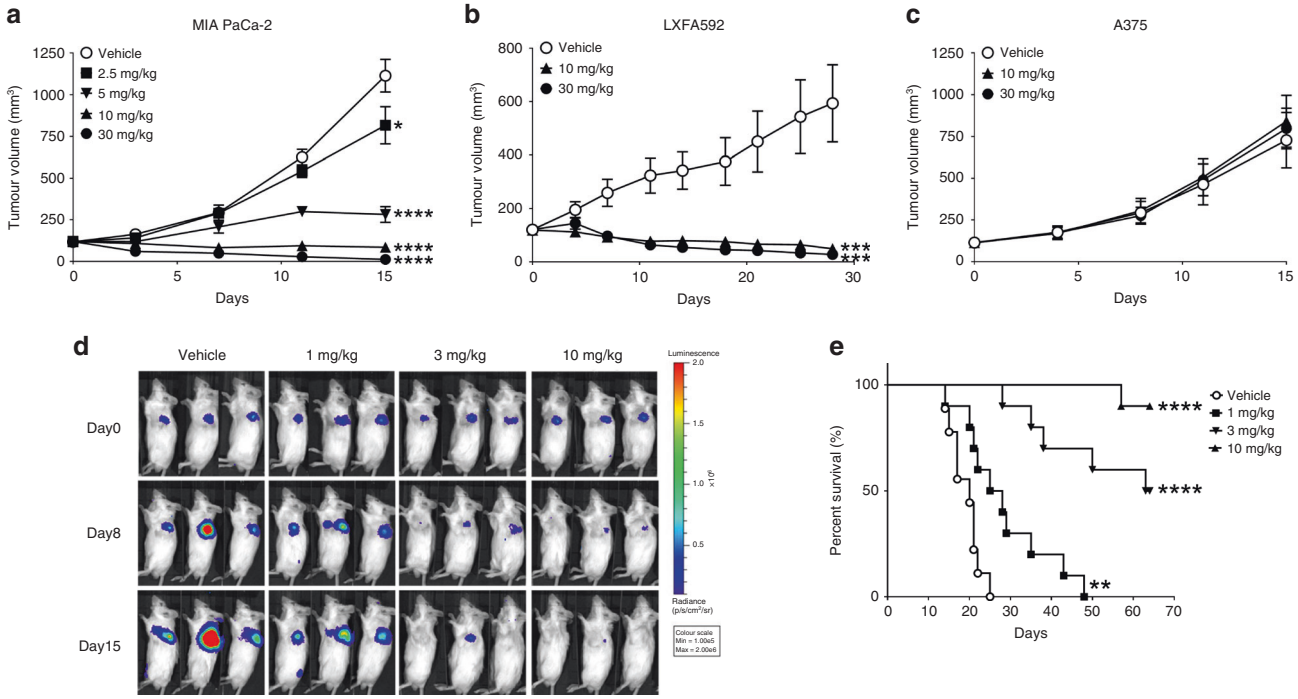

Fig. 4 ASP2453 shows potent anti-tumour activity in multiple human cancer xenograft models. a Anti-tumour activity of ASP2453 in a subcutaneous KRAS G12C-mutated MIA PaCa-2 xenograft model ($n = 5$ mice per group, mean ± SEM). *$P < 0.05$, ****$P < 0.0001$, Dunnett's multiple comparison test compared with vehicle. **b** Anti-tumour activity of ASP2453 in a subcutaneous KRAS G12C-mutated LXFA592 PDX xenograft model (vehicle or 30 mg/kg-treated group: $n = 8$ mice per group, 10 mg/kg-treated group: $n = 7$ mice per group, mean ± SEM). ***$P < 0.001$, Dunnett's multiple comparison test compared with vehicle. **c** Anti-tumour activity of ASP2453 in a subcutaneous KRAS WT A375 xenograft model ($n = 5$ mice per group, mean ± SEM). **d** Bioluminescence imaging of mice orthotopically inoculated with NCI-H1373-Luc cells administered ASP2453. Day 0: day of randomisation. Representative images of 10 mice from each group are shown. **e** Survival of mice orthotopically inoculated with NCI-H1373-Luc cells administered ASP2453 ($n = 10$ mice per group). **$P < 0.01$, ****$P < 0.0001$, two-sided Mantel–Cox test compared with vehicle.

WT A375 xenograft model at 30 mg/kg, the dose at which anti-tumour activity was observed in xenograft models with KRAS G12C mutation (Fig. 4c).

To investigate the effect of ASP2453 in another lung cancer model, we established an orthotopic xenograft model which reflects the tumour microenvironment. NCI-H1373-Luc cells were directly inoculated into the left lung of mice, and tumour formation and progression were monitored using bioluminescence imaging of luciferase activity. In the vehicle-treated group, we detected tumour-derived signal in the lung and the signal was time-dependently progressed (Fig. 4d and Supplementary Fig. S2B). ASP2453 reduced the signal relative to that on day 0, with the signal in ASP2453 (10 mg/kg)-treated mice reaching near-background levels. Further, ASP2453 significantly prolonged the survival of mice (Fig. 4e). Collectively, these results show that ASP2453 KRAS G12C-dependently and selectively induces anti-tumour activity in various xenograft models.

Combination of ASP2453 with erlotinib, trametinib or anti-PD-1 antibody inhibits cell proliferation in vitro and tumour growth in vivo

We examined the effects of ASP2453 in combination with erlotinib, trametinib and anti-programmed cell death 1 (PD-1) antibody in vitro and in vivo to consider the effective combination to improve clinical efficacy and overcome treatment resistance. EGF weakened the anti-proliferative effect of ASP2453, but the combination of ASP2453 with erlotinib, an EGFR inhibitor, potentiated the inhibitory activity on cell proliferation in the presence of added EGF in NCI-H358 cells (Fig. 5a). Co-treatment comprising trametinib and ASP2453 potentiated the inhibitory effect on proliferation of NCI-H358 cells compared with single treatment (Supplementary Fig. S3A). In the NCI-H358 xenograft model, while single treatment with ASP2453 or erlotinib showed significant anti-tumour efficacy, and the efficacy of erlotinib was improved by combined treatment with ASP2453 without significant body weight loss (Fig. 5b and Supplementary Fig. S3B). Similarly, co-administration of trametinib with ASP2453 showed more potent anti-tumour efficacy than single treatment with trametinib without significant body weight loss (Supplementary Fig. S3C, D).

We next investigated the anti-tumour effect of treatment with ASP2453 and anti-PD-1 antibody in a mouse syngeneic model. CT26.WT_mKRAS (p.G12C) (KI) cells were generated using the CRISPR-Cas9 system and showed sensitivity to ASP2453 in vitro (Supplementary Fig. S3E). A single treatment with ASP2453 induced tumour growth regression and prolonged survival in CT26.WT_mKRAS (p.G12C) (KI) syngeneic mice (Fig. 5c and Supplementary Fig. S3F). Co-administration of ASP2453 with anti-PD-1 antibody-induced complete tumour regression at day 56 (three or four of ten mice receiving 20 or 30 mg/kg of ASP2453 plus anti-PD-1 treatment, respectively), and significantly prolonged survival of mice compared with single ASP2453 treatment. Based on these data, ASP2453 in combination with an EGFR, MEK or immune checkpoint inhibitor may be efficacious in tumours expressing KRAS G12C mutations.

Comparison of binding mode, kinetics and inhibitory activity between ASP2453 and AMG 510 in vitro and in vivo

To further understand the inhibitory activity of ASP2453 against mutated KRAS at the structural level, we performed computational modelling of KRAS G12C bound to ASP2453 [22] (Fig. 6a, left). The modelling suggested that ASP2453 fits into the allosteric binding

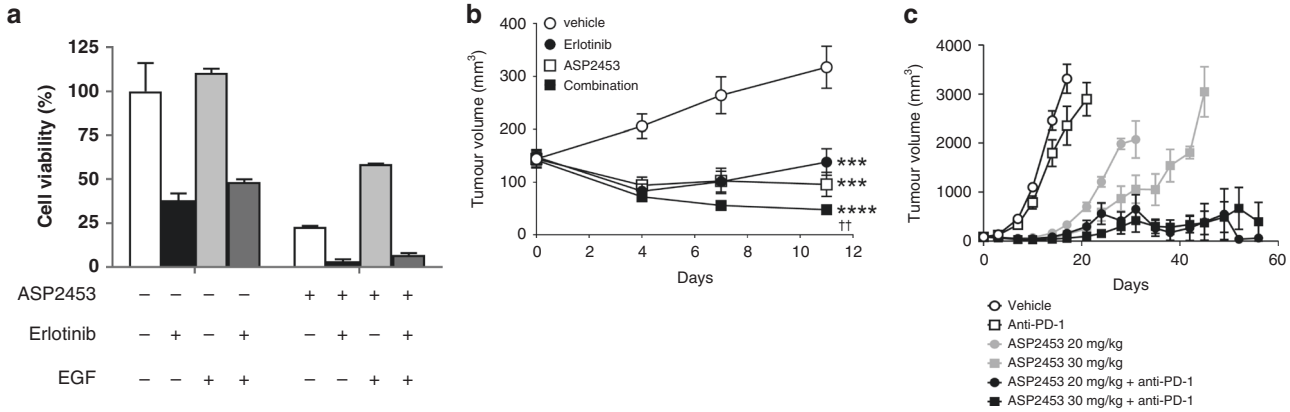

Fig. 5 Combination ASP2453 with erlotinib or anti-PD-1 antibody inhibits cell proliferation in vitro and tumour growth in vivo. **a** Combination ASP2453 (1 nmol/L) with erlotinib (500 nmol/L) under EGF stimulation (0.1 ng/mL) inhibits the proliferation of KRAS G12C-mutated NCI-H358 cells in 3D spheroid culture (mean ± SD). **b** Anti-tumour activity of ASP2453 (10 mg/kg) in combination with erlotinib (100 mg/kg) in a subcutaneous NCI-H358 xenograft model ($n = 5$ mice per group, mean ± SEM). ***$P < 0.01$, ****$P < 0.001$, Dunnett's multiple comparison test compared with vehicle. $^{††}P < 0.01$, two-tailed Student's *t*-test compared with erlotinib-treated group. **c** Anti-tumour activity of ASP2453 in combination with anti-PD-1 antibody in a subcutaneous CT26.WT_mKRAS (p.G12C) (KI) syngeneic model ($n = 5$ mice per group, mean ± SEM).

pocket of KRAS G12C near the GDP-binding site, a finding that was also recently discovered for other KRAS G12C inhibitors [13]. We compared the binding mode of ASP2453 with that of AMG 510 [15] (Fig. 6a, right). We found that ASP2453 interacts with KRAS G12C in a deeper and broader manner than AMG 510. ASP2453 interacts with two extended interaction regions; one is composed of Tyr64 and Gln99, another is composed of Lys88 and Asp92. The model also suggested that the covalent binding site of ASP2453 with Cys12 is closer than AMG 510 by the length of one carbon atom.

To determine whether there are any other differences between ASP2453 and AMG 510, we investigated their binding kinetics to KRAS G12C. The kinetics of ASP2453 and AMG 510 with KRAS G12C-GDP protein were investigated in a cell-free system using SPR analysis. ASP2453 and AMG 510 are bound to KRAS G12C-GDP in a time-dependent manner (Fig. 6b). Comparison of these compounds at 100 nmol/L showed that the covalent interaction between ASP2453 and KRAS G12C-GDP reached a maximum RU value at ~300 s, while the interaction between AMG 510 and KRAS G12C-GDP reached about half of the maximum RU value at 600 s. These data indicate that ASP2453 more rapidly and potently interacts with KRAS G12C protein than AMG 510.

We further investigated the inhibitory activity of ASP2453 and AMG 510 on KRAS G12C-mediated signal transduction in cells. Inhibition of KRAS activation and induction of the mobility shift of KRAS by ASP2453 in MIA PaCa-2 cells was approximately 10-fold more potent than that by AMG 510 (Supplementary Figs. S1A and S4A). ASP2453 showed faster onset of KRAS-GTP suppression, from 0.5 h at 10 nmol/L and from 2 h at 1.0 nmol/L, than AMG 510, which inhibited KRAS activation from 1 h at 100 nmol/L and from 6 h at 10 nmol/L (Fig. 6c). We evaluated whether the faster onset of KRAS-GTP suppression affects the duration of suppression after washout. The inhibitory effect of ASP2453 on KRAS activation was sustained for 24 h after washout (Fig. 6d). In contrast, AMG 510 inhibited KRAS activation for 6 h, and the inhibitory effect was weakened at 24 h after washout. ASP2453 also showed longer inhibition of p-ERK 1/2 and p-S6 compared with AMG 510. We also assessed the duration of the inhibitory effect of ASP2453 on cell proliferation. Sustained anti-proliferative effects of ASP2453 were observed after washout from 6- or 24-h in treated MIA PaCa-2 (Fig. 6e) and NCI-H1373 cells (Supplementary Fig. S4B). Interestingly, the inhibitory effects of AMG 510 on cell proliferation were significantly weakened after washout.

We next investigated the anti-tumour efficacy of ASP2453 and AMG 510 in a MIA PaCa-2 xenograft model. ASP2453 completely inhibited tumour growth, with three of five mice showing complete tumour regression at day 42. While AMG 510 also significantly and dose-dependently inhibited tumour growth, no mice showed complete tumour regression at day 42 (Fig. 6f). Moreover, AMG 510 (30 mg/kg) administration for 28 days caused tumour regrowth, and tumour enlargement was observed even after continued AMG 510 administration. Switching from AMG 510 to ASP2453 induced tumour regression relative to the tumour volume on day 28, while switching to a higher dose of AMG 510 resulted in only tumour growth inhibition in AMG 510-resistant mice without affecting body weight (Fig. 6g and Supplementary Fig. S4C). Taken together, these data show that ASP2453 and AMG 510 display differences in binding kinetics, maximum potency and anti-tumour efficacy.

DISCUSSION

KRAS G12C mutation is found in various cancers, particularly in lung adenocarcinoma, suggesting that inhibitors of KRAS G12C may be potential therapeutic agents for cancer patients with KRAS G12C mutations. Previous studies have shown that inhibitors that covalently bind to the cysteine at residue 12 of KRAS selectively inhibit KRAS signal transduction, cell proliferation and tumour growth in KRAS G12C-mutated cancer cells or tumours [13–15, 17, 22, 23]. In this report, we investigated the anti-tumour activity of ASP2453, our novel KRAS G12C inhibitor, in KRAS G12C-mutated cancers. ASP2453 covalently and selectively interacted with KRAS G12C, and selectively inhibited the proliferation of KRAS G12C-mutated cancer cells, with inhibition of KRAS activation and downstream signalling across KRAS-mutated or WT cell line panels. Once-daily oral administration of ASP2453 resulted in tumour regression in KRAS G12C-mutated CDX and PDX models. This anti-tumour activity was associated with inhibition of KRAS activation, p-ERK 1/2 and p-S6 in response to increasing intratumor concentrations of ASP2453. Furthermore, ASP2453 treatment prolonged the survival of orthotopic xenograft model mice.

The molecular mechanisms of KRAS signalling are complicated because of the presence of many positive and negative feedback signals and crosstalk pathways. The efficacy of inhibitors targeting KRAS signalling molecules such as EGFR and MEK are limited and treatment resistance frequently occurs due to bypass signalling

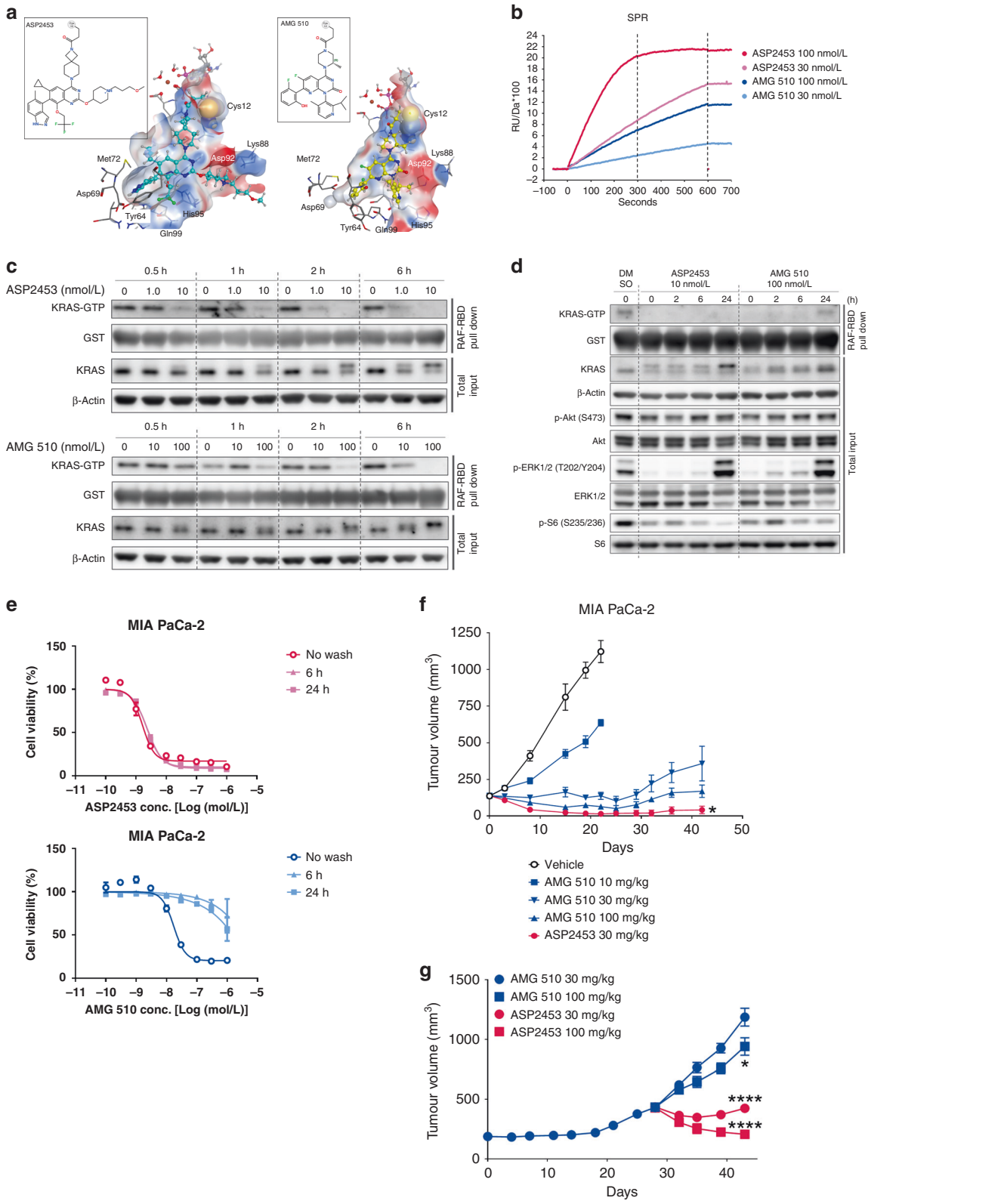

activations and resistance mutations develop. Strategies to combine treatment with these inhibitors have been widely investigated to maximise clinical efficacy and overcome treatment resistance in KRAS-mutated cancer. KRAS G12C inhibitors have also been investigated in combination with various other targeted agents involved in RTK, SHP2, MEK1/2, mTOR and CDK4/6 inhibition [15, 23, 24]. EGF weakened the inhibitory effects of ARS-853 via EGFR activation, but co-treatment with ARS-853 and erlotinib, an EGFR inhibitor, enhanced the in vitro anti-proliferative effects under EGF stimulation [23]. Combining AMG 510 and trametinib, a MEK inhibitor, enhanced the anti-tumour effect in heterozygous KRAS G12C-mutated NCI-H358 tumours [15]. In the

Fig. 6 Comparison of ASP2453 and AMG 510 in vitro and in vivo. a Chemical structures and binding modes of ASP2453 (left) and AMG 510 (right). Chemical structures are shown in the insets. ASP2453, AMG 510, GDP, Mg^{2+} ion, and water molecules bound to the Mg^{2+} ion are shown as ball-and-stick figures and other atoms are shown as sticks. Each element is represented by a different colour (white: hydrogen, cyan or grey: carbon, blue: nitrogen, red: oxygen, yellow: sulfur). The colours of the protein surfaces are based on electrostatic potential (blue: positive, red: negative, white: neutral). For clarity, non-polar hydrogen atoms have been omitted and the protein surfaces at the front of ASP2453 and AMG 510 are hidden. **b** SPR sensorgram results for the association of ASP2453 and AMG 510 to KRAS G12C-GDP protein. **c** Time course of KRAS activation and KRAS mobility shift in MIA PaCa-2 cells. MIA PaCa-2 cells were treated with ASP2453 or AMG 510 for the indicated period of time. KRAS activation and KRAS mobility shift were detected using a RAF-RBD pulldown assay and immunoblotting. **d** Time course of KRAS activation, KRAS mobility shift and downstream signals in MIA PaCa-2 cells after removal of ASP2453 and AMG 510. MIA PaCa-2 cells were treated with ASP2453 or AMG 510 for 2 h. After treatment, each well was washed three times with medium and incubated for 0, 2, 6 or 24 h. KRAS activation, KRAS mobility shift and downstream signals were detected using a RAF-RBD pulldown assay and immunoblotting. **e** Inhibitory activity of ASP2453 and AMG 510 on the proliferation of MIA PaCa-2 cells after washout (mean ± SD). **f** Anti-tumour activity of ASP2453 and AMG 510 in a subcutaneous KRAS G12C-mutated MIA PaCa-2 xenograft model ($n = 5$ mice per group, mean ± SEM). *$P < 0.05$, Dunnett's multiple comparison test compared with AMG 510 (30 mg/kg)-treated group. **g** Anti-tumour activity of ASP2453 and AMG 510 in an AMG 510-resistant MIA PaCa-2 xenograft model (mean ± SEM). AMG 510 (30 mg/kg) was orally administered once a day for 28 days. Mice were randomised into four groups ($n = 5$) based on tumour volume and ASP2453 or AMG 510 was administered orally once a day. *$P < 0.05$, ****$P < 0.0001$, Dunnett's multiple comparison test compared with AMG 510 (30 mg/kg)-treated group.

present study, combined treatment with ASP2453 showed more potent anti-tumour effects than single treatment of erlotinib or trametinib both in vitro and in vivo.

A recent study reported the promise of immune checkpoint inhibitor therapies such as anti-PD-1 antibody as therapeutic options for patients with NSCLC [25]. Preclinical data shows that co-administration of AMG 510 and anti-PD-1 antibody also significantly improves survival and complete response. A single treatment with ASP2453 induced tumour regression and prolonged survival in a CT26.WT_mKRAS (p.G12C) (KI) mouse syngeneic model. Furthermore, co-administration of ASP2453 with anti-PD-1 antibody significantly prolonged survival. That ASP2453 shows similar combinatory effects with anti-PD-1 antibody to other KRAS G12C inhibitors supports the use of combination treatment with KRAS G12C inhibitors and immune checkpoint inhibitors. These results support the potential rationale of KRAS G12C inhibitors for the use of combination therapy with targeted agents or anti-PD-1 antibody in clinical settings.

Finally, we conducted head-to-head studies comparing the anti-tumour effects of ASP2453 and AMG 510, an FDA-approved compound, in a MIA PaCa-2 xenograft model. ASP2453 induced complete tumour regression at 30 mg/kg, and AMG 510 did not at 100 mg/kg. While long-term administration of AMG 510 at 30 mg/kg led to tumour regrowth, ASP2453 induced tumour regression in AMG 510-resistant tumours. We compared ASP2453 and AMG 510 in in vitro experiments and identified two main differences: potency of inhibitory activity in cells and binding kinetics to KRAS G12C protein. ASP2453 had approximately 10-fold more potent KRAS activation and cell growth inhibitory activity than AMG 510. Further, SPR analysis and washout experiments showed that ASP2453 bound to KRAS G12C protein faster and for longer periods than AMG 510. That displacement of interactions between protein and a bound ligand with other molecules like water is involved in the dissociation process of a bound ligand [26, 27] suggests that a number of favourable interactions attenuate the dissociation of small molecules from the binding pocket. Therefore, the broader interaction area of ASP2453 suggested by our computational analysis [22] may contribute to the slower dissociation of ASP2453 compared with AMG 510. In addition, glutathione (GSH) adduct experiments showed that the covalent region of ASP2453 may be more reactive than that of AMG 510 [28]. In addition to the slower dissociation, this may also contribute to the faster onset of ASP2453. These characteristics of ASP2453 are consistent with the experimental results described above. Collectively, our data suggest that, despite having similar modes of action, differences in potency and onset of efficacy between ASP2453 and AMG 510 may cause differences in the duration of anti-tumour efficacy and acquisition of drug resistance. Additional research is needed on the molecular mechanisms of ASP2453 on AMG 510-resistance.

In summary, we identified an orally available, highly potent and selective KRAS G12C covalent inhibitor, ASP2453, which elicits potent anti-tumour activity in various preclinical models harbouring KRAS G12C mutations and AMG 510-resistant xenograft models, likely due to its high potency and fast onset. Our data show that ASP2453 monotherapy and combination treatment is well tolerated in mice and efficacious in tumour xenograft models that are insensitive or refractory to AMG 510.

DATA AVAILABILITY

Researchers may request access to anonymized participant-level data, trial-level data and protocols from Astellas sponsored clinical trials at www.clinicalstudydatarequest.com. For the Astellas criteria on data sharing see https://clinicalstudydatarequest.com/Study-Sponsors/Study-Sponsors-Astellas.aspx.

REFERENCES

1. Wennerberg K, Rossman KL, Der CJ. The Ras superfamily at a glance. J Cell Sci. 2005;118:843–6.
2. Ryan MB, Corcoran RB. Therapeutic strategies to target RAS-mutant cancers. Nat Rev Clin Oncol. 2018;15:709–20.
3. Pylayeva-Gupta Y, Grabocka E, Bar-Sagi D. RAS oncogenes: weaving a tumorigenic web. Nat Rev Cancer. 2011;11:761–74.
4. Cox AD, Fesik SW, Kimmelman AC, Luo J, Der CJ. Drugging the undruggable RAS: Mission possible? Nat Rev Drug Discov. 2014;13:828–51.
5. Hunter JC, Manandhar A, Carrasco MA, Gurbani D, Gondi S, Westover KD. Biochemical and structural analysis of common cancer-associated KRAS mutations. Mol Cancer Res. 2015;13:1325–35.
6. Guerrero S, Casanova I, Farré L, Mazo A, Capellà G, Mangues R. K-*ras* codon 12 mutation induces higher level of resistance to apoptosis and predisposition to anchorage-independent growth than codon 13 mutation or proto-oncogene overexpression. Cancer Res. 2000;60:6750–6.
7. Cancer Genome Atlas Research Network. Comprehensive molecular profiling of lung adenocarcinoma. Nature. 2014;511:543–50.
8. Ferlay J, Soerjomataram I, Dikshit R, Eser S, Mathers C, Rebelo M, et al. Cancer incidence and mortality worldwide: sources, methods and major patterns in GLOBOCAN 2012. Int J Cancer. 2015;136:E359–386.
9. Siegel RL, Miller KD, Jemal A. Cancer statistics, 2020. CA Cancer J Clin. 2020; 70:7–30.
10. Ahrendt SA, Decker PA, Alawi EA, Zhu Y-r, Sanchez-Cespedes M, Yang SC, et al. Cigarette smoking is strongly associated with mutation of the K-ras gene in patients with primary adenocarcinoma of the lung. Cancer. 2001;92:1525–30.
11. Dogan S, Shen R, Ang DC, Johnson ML, D'Angelo SP, Paik PK, et al. Molecular epidemiology of EGFR and KRAS mutations in 3,026 lung adenocarcinomas: higher susceptibility of women to smoking-related KRAS-mutant cancers. Clin Cancer Res. 2012;18:6169–77.
12. Nadal E, Chen G, Prensner JR, Shiratsuchi H, Sam C, Zhao L, et al. KRAS-G12C mutation is associated with poor outcome in surgically resected lung adenocarcinoma. J Thorac Oncol. 2014;9:1513–22.

13. Ostrem JM, Peters U, Sos ML, Wells JA, Shokat KM. K-Ras(G12C) inhibitors allosterically control GTP affinity and effector interactions. Nature. 2013;503:548–51.
14. Lim SM, Westover KD, Ficarro SB, Harrison RA, Choi HG, Pacold ME, et al. Therapeutic targeting of oncogenic K-Ras by a covalent catalytic site inhibitor. Angew Chem Int Ed Engl. 2014;53:199–204.
15. Canon J, Rex K, Saiki AY, Mohr C, Cooke K, Bagal D, et al. The clinical KRAS(G12C) inhibitor AMG 510 drives anti-tumour immunity. Nature. 2019;575:217–23.
16. Lanman BA, Allen JR, Allen JG, Amegadzie AK, Ashton KS, Booker SK, et al. Discovery of a covalent inhibitor of KRAS(G12C) (AMG 510) for the treatment of solid tumors. J Med Chem. 2020;63:52–65.
17. Hallin J, Engstrom LD, Hargis L, Calinisan A, Aranda R, Briere DM, et al. The KRAS(G12C) inhibitor MRTX849 provides Insight toward therapeutic susceptibility of KRAS-mutant cancers in mouse models and patients. Cancer Disco. 2020;10:54–71.
18. Hong DS, Fakih MG, Strickler JH, Desai J, Durm GA, Shapiro GI, et al. KRAS (G12C) inhibition with sotorasib in advanced solid tumors. N. Engl J Med. 2020;383:1207–17.
19. Jänne, PA, Rybkin, II, Spira, AI, Riely, GJ, Papadopoulos, KP, Sabari, JK, et al. KRYSTAL-1: activity and safety of adagrasib (MRTX849) in advanced/metastatic non–small-cell lung cancer (NSCLC) harboring KRAS G12C mutation. Presented at the 2020 AACR-NCI-EORTC meeting (2020).
20. Johnson, ML, Ou, SHI, Barve, M, Rybkin, II, Papadopoulos, KP, Leal, TA, et al. KRYSTAL-1: activity and safety of adagrasib (MRTX849) in patients with colorectal cancer (CRC) and other solid tumors harboring a KRAS G12C mutation. Presented at the 2020 AACR-NCI-EORTC meeting (2020).
21. Kim D, Xue JY, Lito P. Targeting KRAS(G12C): from inhibitory mechanism to modulation of antitumor effects in patients. Cell. 2020;183:850–9.
22. Janes MR, Zhang J, Li LS, Hansen R, Peters U, Guo X, et al. Targeting KRAS mutant cancers with a covalent G12C-specific inhibitor. Cell. 2018;172:578–89. e517
23. Patricelli MP, Janes MR, Li LS, Hansen R, Peters U, Kessler LV, et al. Selective inhibition of oncogenic KRAS output with small molecules targeting the inactive state. Cancer Discov. 2016;6:316–29.
24. Molina-Arcas M, Moore C, Rana S, van Maldegem F, Mugarza E, Romero-Clavijo P, et al. Development of combination therapies to maximize the impact of KRAS-G12C inhibitors in lung cancer. Sci Transl Med. 2019;11:eaaw7999.
25. Ribas A, Wolchok JD. Cancer immunotherapy using checkpoint blockade. Science. 2018;359:1350–5.
26. Tiwary P, Limongelli V, Salvalaglio M, Parrinello M. Kinetics of protein–ligand unbinding: predicting pathways, rates, and rate-limiting steps. Proc Natl Acad Sci USA. 2015;112:E386–91.
27. Copeland RA. The drug–target residence time model: a 10-year retrospective. Nat Rev Drug Discov. 2016;15:87–95.
28. Palkowitz MD, Tan B, Hu H, Roth K, Bauer RA. Synthesis of diverse N-acryloyl azetidines and evaluation of their enhanced thiol reactivities. Org Lett. 2017;19:2270–3.

ACKNOWLEDGEMENTS

We thank Dr Hirofumi Ishii, Dr Yukinori Shimoshige and Mr Yosuke Yamanaka for support with the biological study. We are grateful to Dr Masahiko Hayakawa and Dr Taku Yoshida for their useful suggestions.

AUTHOR CONTRIBUTIONS

AN, TN and MS conceived the study and designed experiments. AN, YN, TN, MS, KK, KM, KH and MY developed methodology. AN, YN, TN, KK, KM, KH and MY acquired and analysed the data. All authors edited the manuscript and approved the submission of the final version.

FUNDING

This study was funded by Astellas Pharma Inc.

ETHICS APPROVAL AND CONSENT TO PARTICIPATE

No human participants, human data or human tissue were used as parts of this study. All animal experimental procedures were approved by the Institutional Animal Care and Use Committee of Astellas Pharma Inc., Tsukuba Research Center, which is accredited by AAALAC International.

CONSENT FOR PUBLICATION

Not applicable.

COMPETING INTERESTS

All authors are employees of Astellas Pharma Inc. and its affiliates.

ADDITIONAL INFORMATION

Supplementary information The online version contains supplementary material available at https://doi.org/10.1038/s41416-021-01629-x.

Correspondence and requests for materials should be addressed to Ayako Nakayama.